Article

Multiplex Optical Urinalysis for Early Detection of Drug-induced Kidney Injury

Penghui Cheng, Qingqing Miao, Jiaguo Huang, Jingchao Li, and Kanyi Pu

Anal. Chem., **Just Accepted Manuscript** • DOI: 10.1021/acs.analchem.0c00989 • Publication Date (Web): 02 Apr 2020

Multiplex Optical Urinalysis for Early Detection of Drug-induced Kidney Injury

Penghui Cheng, Qingqing Miao, Jiaguo Huang, Jingchao Li and Kanyi Pu*

School of Chemical and Biomedical Engineering, Nanyang Technological University, 637457 Singapore. Email: kypu@ntu.edu.sg

ABSTRACT: Drug-induced kidney injury (DIKI) is a significant contributor of both acute and chronic kidney injury, and remains a major concern in drug development and clinical care. However, current clinical diagnostic methods often fail to accurately and timely detect nephrotoxicity. This study reports the development of activatable molecular urinary reporters (MURs) that are able to specifically detect urinary biomarkers including γ-glutamyl transferase (GGT), alanine aminopeptidase (AAP) and N-acetyl-β-D-glucosaminidase (NAG). By virtue of their discrete absorption and emission properties, the mixture of MURs can serve as a cocktail sensor for multiplex optical urinalysis in the mouse models of drug-induced acute kidney injury (AKI) and chronic kidney disease (CKD). The MURs cocktail not only detects nephrotoxicity earlier than the tested clinical diagnostic methods in drug-induced AKI and CKD mice models, but also possesses a higher diagnostic accuracy. Therefore, MURs hold great promise for detection of kidney function in both pre-clinical drug screening and clinical settings.

Kidney is a vital organ in the body that plays important roles in regulating body fluid homeostasis and blood filtration as well as maintaining electrolyte balance. As it is the primary site for metabolism and excretion of drugs, imaging contrast agents and environmental hazards, it is vulnerable to the exposure of these toxicants.[1] In particular, drug-induced kidney injury (DIKI) is a frequent complication in intensive care unit (ICU) and has a high risk of morbidity and mortality.[2] Moreover, DIKI remains a significant contributor to acute kidney injury (AKI) and underlines 19-25% of all cases in critically ill patients.[3] Therefore, development of sensitive detection methods for DIKI is of great importance for pharmaceutical companies to screen nephrotoxic drugs in drug development process, and for clinicians to closely monitor patient safety in clinical care.

Current clinical diagnosis often relies on measurement of serum creatinine (sCr) and blood urea nitrogen (BUN), which are factors reflecting changes in glomerular filtration rate (GFR).[4] However, sCr/BUN methods not only fail to sensitively detect kidney injury because substantial histological injuries could occur before measurable GFR change,[5] but also lack in accuracy because patients' age and muscle mass can cause fluctuations in the biomarker levels.[6] In contrast, urinalysis using the biomarkers such as clusterin, Cystatin-C and β2-microglobulin has recently shown to be more sensitive and reliable than clinical diagnostic methods for detection of DIKI in animal studies.[7] However, the detection methods for these urinary biomarkers are limited to commercial immunoassays and matrix-assisted laser desorption ionization time of flight mass spectroscopy (MALDI-TOF-MS). Commercial immunoassays generally suffer from low sensitivity and tedious measurement procedures;[8] MALDI-TOF-MS is a highly specific method in biomarker detection, but its application has been limited by number of reference MS spectra in the database.[9]

Activatable fluorescent probes that specifically emit signals in response to the biomarker of interest have become indispensable tools in fundamental biology,[10-12] and medical applications.[13-16] With a high signal-to-background ratio, fluorescent probes often have high sensitivity and strong ability for early detection of diseases such as cancer,[17-20] skin diseases,[21,22] acute liver injury[23-25] and diabetes.[26] Additionally, multiplex fluorescence imaging provides a unique approach to simultaneously study multiple interrelated biomarkers at the same time, potentially improving diagnostic accuracy.[27,28] However, activatable fluorescent probes have been less exploited for detection of DIKI,[29-31] not to mention multiplex fluorescence imaging.

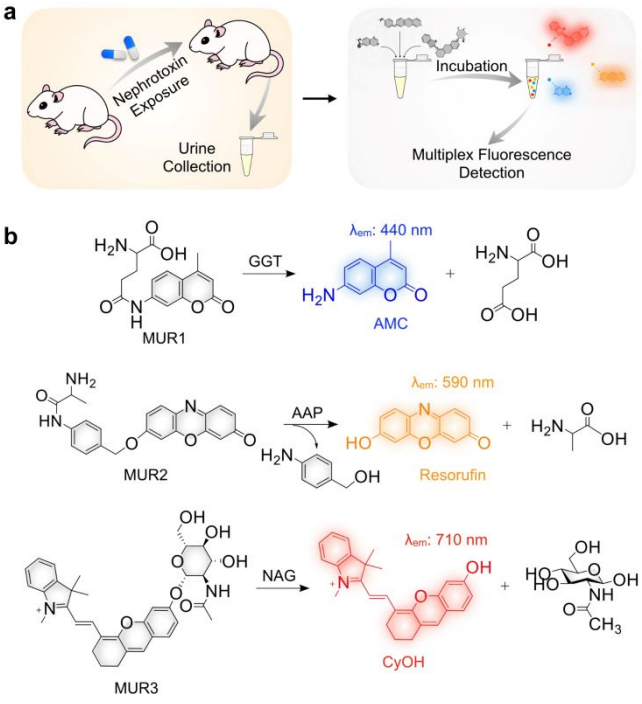

Scheme 1. Design and urinalysis mechanism of MURs. (a) Multiplex optical urinalysis mechanism of MURs. (b) Molecular structures and sensing mechanisms of MURs towards urinary biomarkers.

In this study, we report the development of three molecular urinary reporters (MURs) for multiplex optical urinalysis in early detection of DIKI. Because elevated urinary excretion of proximal tubule brush border enzymes (γ-glutamyl transferase: GGT; alanine aminopeptidase: AAP) and lysosomal enzyme (N-acetyl-D-glucosamine: NAG) has been found at the early stage of both glomerulonephritis[32] and acute tubular necrosis,[33] they are chosen as the DIKI biomarkers for the design of MURs. Activatable molecular fluorophores responsive towards GGT,[34-36] AAP,[37] and NAG[38,39] have been previously reported, the molecules are designed by caging the fluorophore optically-tunable atoms (typically oxygen or nitrogen) with an enzyme cleavable moiety. However, they were not applied for multiplex imaging. MURs1-3 are devised to emit blue, orange and near-infrared (NIR) fluorescence signals upon activation by GGT, AAP, and NAG, respectively. Due to the minimal spectral overlap, MURs1-3 can form a cocktail sensor for multiplex optical urinalysis of DIKI.

Experimental Section

Materials

All chemicals were purchased from Sigma-Aldrich unless otherwise stated. Commercially available reagents were used without further purification unless otherwise noted. Fmoc-Ala-OH was purchased from Sangon Biotech. Alanine aminopeptidase (AAP), fibroblast activation protein-alpha (FAP-α), furin, matrix metalloproteinase-2 (MMP2), and dipeptidyl peptidase-4 (DPP4) were purchased from R&D Systems.

Instrumentation

UV/Vis spectra were measured on a Shimadzu UV-2450 spectrophotometer. Fluorescence measurements were performed on a Fluorolog 3-TCSPC spectrofluorometer (Horiba Jobin Yvon). HPLC analyses were done on an Agilent 1260 system equipped with a G1311B pump, UV detector and an Agilent Zorbax SB-C18 RP (9.4 × 250 mm) column, with methanol (0.1% CF_3COOH) and water (0.1% CF_3COOH) as the eluent. Fluorescence images of living cells and immunofluorescent imaging of kidney slices were acquired on Laser Scanning Microscope LSM800 (Zeiss). Proton-nuclear magnetic resonance (^1H NMR) spectra were recorded on a Bruker Advance II 300 MHz NMR. Electrospray ionization-mass spectrometry (ESI-MS) spectra were acquired on a Thermo Finnigan Polaris Q quadrupole ion trap mass spectrometer (ThermoFisher Corporation) equipped with a standard ESI source.

Syntheses

Synthesis of Compound 1. Fmoc-Ala-OH (310 mg, 1 mmol), p-aminobenzyl alcohol (250 mg, 2 mmol) and N-Ethoxycarbonyl-2-ethoxy-1,2-dihydroquinoline (300 mg, 2 mmol) were dissolved and mixed in anhydrous dichloromethane (DCM) and stirred overnight under N_2 atmosphere. The organic solvent was concentrated under reduced pressure. After HPLC purification, pure compound 1 could be obtained (330 mg, 0.8 mmol). ^1H NMR (300 MHz, $CDCl_3$) δ: 7.76 (d, J = 6 Hz, 2H), 7.57 (d, J = 6 Hz, 2H), 7.47 (d, J = 9 Hz, 2H), 7.39 (t, 2H), 7.30 (d, J = 9 Hz, 4H), 4.65 (s, 2H), 4.46 (d, J = 6 Hz, 2H), 4.36 (s, 1H), 4.21 (t, 1H), 1.46 (d, J = 6 Hz, 3H). MS (ESI): m/z = 417.24 $[M + H]^+$.

Synthesis of compound 2. Pure compound 1 (100 mg, 0.25 mmol) was dissolved in anhydrous tetrahydrofuran (THF) in ice bath under N_2 atmosphere, and PBr_3 (37 μL, 0.38 mmol) in anhydrous THF was added via a syringe. The reaction mixture was stirred for 2 h before the solvent was concentrated under reduced pressure. The resulting mixture was diluted with ethyl acetate and washed with saturated sodium bicarbonate solution for three times to remove residual acid. The organic layer was dried was anhydrous sodium sulfate and concentrated under reduced pressure. The crude product was then taken for next step synthesis without further purification.

Synthesis of compound 3. Resorufin (10 mg, 0.05 mmol) and grinded potassium carbonate (25 mg, 0.2 mmol) were vigorously stirred in anhydrous dimethylformamide (DMF) under N_2 atmosphere for 30 minutes, before compound 2 (95 mg, 0.2 mmol) dissolved in anhydrous DMF was added via a syringe. The mixture was continuously stirred for 5 h, and then pure compound 3 (29 mg, 95%) could be obtained after HPLC purification. ^1H NMR (300 MHz, DMSO-d6) δ: 7.89 (d, J = 6 Hz, 2H), 7.63-7.79 (m, 6H), 7.53 (d, J = 12Hz, 1H), 7.42 (m, 3H), 7.32 (m, 2H), 7.18 (d, J = 3 Hz, 1H), 7.12 (m, 1H), 6.78 (m, 1H), 6.27 (d, J = 2.1 Hz, 1H), 5.22 (s, 2H), 4.24 (m, 4H), 1.30 (d, J = 7 Hz, 3H). MS (ESI): m/z = 611.75 $[M + H]^+$.

Synthesis of MUR2. Pure compound 3 (20 mg, 0.03 mmol) was stirred in 5% piperidine/DMF for 10 minutes at rt, before 10-times diluted acetic acid was added dropwise until pH was adjusted to 7. Pure MUR2 (10 mg, 90%) could be obtained after HPLC purification. ^1H NMR (300 MHz, CD_3CN) δ: 7.64 (d, J = 9 Hz, 1H), 7.53 (d, J = 6Hz, 2H), 7.40 (s, 1H), 7.38 (m, 2H), 6.97 (m, 1H), 6.90 (d, J = 3Hz, 1H),6.67 (m, 1H), 6.15 (d, J = 3Hz, 1H), 5.12 (s, 2H), 4.05 (m, 1H), 1.49 (d, J = 6Hz, 3H). MS (ESI): m/z = 389.79 $[M + H]^+$.

Synthesis of CyOH. Synthesis was carried out according to literature report.[40] ^1H NMR (300 MHz, $CDCl_3$) δ: 8.18 (d, J = 15 Hz, 1H), 7.70 (m, 1H), 7.35 (s, 1H), 7.31 (s, 1H), 7.22 (s, 1H), 7.10 (t, 1H), 6.89 (t, 2H), 5.67 (d, J = 12 Hz, 1H), 2.65 (m, 3H), 1.91 (t, 2H), 1.69 (s, 6H), 1.25 (s, 4H), 0.86 (m, 3H). MS (ESI): m/z = 386.45 $[M + H]^+$.

Synthesis of Compound 4. β-D-galactosamine pentaacetate (780 mg, 2 mmol) was dissolved and stirred in 6 mL anhydrous DCM in ice bath under N_2 atmosphere, and HBr (33 wt% in acetic acid, 4.7 mL, 2 mmol) was added via a syringe. The mixture was continuously stirred in ice bath for 6 h. The residue mixture was then washed with ice-cold saturated sodium bicarbonate solution for three times to remove residue acid. The organic layer was dried with anhydrous sodium sulfate and concentrated under reduced pressure. The crude product was stored at -20 °C and directly taken for next step synthesis without further purification. MS (ESI): m/z = 409.71 $[M + H]^+$.

Synthesis of compound 5. Pure CyOH (20 mg, 0.054 mmol) and grinded potassium carbonate (28 mg, 0.2 mmol) was mixed and stirred in anhydrous DCM under N_2 atmosphere for 30 minutes before compound 4 (86 mg, 0.2 mmol) dissolved in anhydrous DCM was added via a syringe. The residue mixture was stirred overnight and concentrated under reduced pressure. The crude product was directly used for next step synthesis without further purification. MS (ESI): m/z = 713.56 $[M + H]^+$.

Synthesis of MUR3. Crude compound 5 (38 mg, 0.054 mmol) and MeONa (25 wt% in methanol [MeOH], 550 μL, 2 mmol) were dissolved and stirred in MeOH in ice bath. The reaction was continuously monitored by thin-layer chromatography, and 10-times diluted acetic acid was added dropwise until pH was adjusted to 7. The residue mixture was concentrated under reduced pressure and purified with column chromatography to yield pure MUR3 (20 mg, 64%). ^{1}H NMR (300 MHz, MeOD) δ: 8.78 (d, J = 15 Hz, 1H), 7.67 (d, J = 8 Hz, 1H), 7.47 (m, 3H), 7.33 (s, 1H), 7.13 (s, 1H), 7.00 (d, J = 9 Hz, 1H), 6.55 (J = 15 Hz, 1H), 5.21 (m, 1H), 3.96 (m, 4H), 3.73 (m, 1H), 3.59 (m, 2H), 3.42 (m, 2H), 2.75 (d, J = 15 Hz, 4H), 1.96 (m, 6H), 1.81 (s, 3H), 1.28 (s, 2H). MS (ESI): m/z = 587.30 $[M + H]^+$.

Enzyme kinetic studies. Various concentrations of MUR1 (10, 20, 40, 80, 160, 320, 640, 800 μM) were incubated with GGT (5 μg) at 37 °C for 5 min in a 100 μL system of PBS buffer (1×, pH = 7.4) with 0.02% Tween@20. Similarly, various concentrations of MUR2 (5, 10, 20, 40, 80, 160, 240, 320 μM) were incubated with AAP (0.1 μg) at 37 °C for 5 min in a 100 μL system of Tris buffer (50 mM, pH = 7.4). Lastly, various concentrations of MUR3 (10, 25, 50, 100, 150, 300, 600 μM) were incubated with NAG (10 mU) at 37 °C for 5 min in a 100 μL system of PBS buffer (1×, pH = 7.4). After incubation, the mixture was injected into HPLC (eluent: methanol/water) for quantification analyses. The initial reaction velocity (μmol/s) was calculated, plotted against MURs1-3 concentration, and fitted to a Michaelis-Menten curve. The kinetic parameters were calculated using Michaelis-Menten equation: $V = V_{max}*[S] (K_M + [S])$, where V is initial velocity, and [S] is substrate concentration.

Cell culture. HK-2 and NDF cells were cultured in Dulbecco's Modified Eagle Media (DMEM) medium supplemented with heat-inactivated fetal bovine serum (10%) and antibiotics penicillin/streptavidin (1%) in a humidified environment containing 5% CO_2 and 95% air at 37 °C. Cell media was replaced every two to three days.

Cell fluorescence imaging. For cell fluorescence imaging, HK-2 and NDF cells (10^5 cells per well in 1 mL) were seeded in the dishes (dia. 35mm) and incubated overnight to reach 80% confluency, respectively. The cells were incubated with 30 μM MURs cocktail (containing 10 μM of each MUR) for 30 minutes. The medium was removed, and the cells were washed with PBS for three times. Then the cells were fixed with 4% polyformaldehyde solution. Fluorescence images of fixed cells were acquired on a Laser Scanning Microscope LSM800 (Zeiss). The excitation and emission wavelength for cell imaging were 405/410-470nm for MUR1, 561/580-630nm for MUR2 and 640/655-710nm for MUR3. ImageJ software was utilized to remove signal background and quantify cellular fluorescence intensity.

Cytotoxicity assay. HK-2 and NDF cells were seeded in 96-well plates (10^4 cells per well) for 24 h, and then different concentrations of MUR cocktail (5, 10, 20, 30 and 40 μM, containing equimolar amount of each MUR) were added to the cell culture medium. Cells were incubated with or without (control) MUR cocktail, followed by addition of MTS assay (Promega Cat. no. G3581, 100 mL, 0.1 mg/mL) for 4 h. The absorbance of MTS at 490 nm was measured by using a microplate reader. The cytotoxic effects (VR) of MUR cocktail were assessed using the following equation: $VR = A/A_0 \times 100\%$, where A and A_0 are the absorbance of the experimental group and control group, respectively. The assays were performed in five sets for each concentration.

Mice cisplatin-induced acute kidney injury model development. All animal experiments were performed in accordance with the Guidelines for Care and Use of Laboratory Animals of the Nanyang Technological University-Institutional Animal Care and Use Committee (NTU-IACUC) and approved by the Institutional Animal Care and Use Committee (IACUC) for Animal Experiment, Singapore. The choice of drug dosage and injection methods could be found in literature reports. Cisplatin (1 mg/mL in 0.9% NaCl solution) was injected once intraperitoneally into Ncr mice (18-20 g, drug dosage 20 mg/kg bw). Age-matched control Ncr mice were injected with an equal volume of isotonic saline. All mice were housed in a temperature controlled (22 °C) room with 12 h dark light cycles (0700 h on and 1900 h off). All mice were weighed twice daily. Mice were sacrificed at different drug post-treatment time points (t = 12, 24, 48 and 72 h). An overnight urine collection of spontaneously voided urine was made from each animal in metabolic cages on the night before sacrifice. Blood samples for serum creatinine (sCr) and Blood Urea Nitrogen (BUN) were obtained from central tail artery in non-anesthetized mice. Obtained blood samples were stored in ice and centrifuged at 3000 rpm for 10 minutes to separate serum.

Mice doxorubicin-induced chronic kidney injury model development. The choice of drug dosage and injection methods could be found in literature reports. Doxorubicin (1 mg/mL in 0.9% NaCl solution) was intravenously injected into BALB/c mice (18-20 g, 10 mg/kg bw). Age-matched control BALB/c mice were injected with an equal volume of isotonic saline. All mice were housed in a temperature controlled (22 °C) room with 12 h dark light cycles (0700 h on and 1900 h off). All mice were weighed twice daily. Mice were sacrificed at different drug post-treatment time points (t = 5, 8, 10, 14, 21, 28 days). An overnight urine collection of spontaneously voided urine was made from each animal in metabolic cages on the night before sacrifice. Blood samples for serum albumin and creatinine (Cr) were obtained from central tail artery in non-anesthetized mice. Obtained blood samples were stored in ice and centrifuged at 3000 rpm for 10 minutes to separate serum.

Statistics analysis. Statistical comparisons between the two groups were determined by Student's t-test (1-tailed, unpaired). For all tests, $p < 0.05$ was considered as statistically significant. For analysis of diagnostic performance of MURs, ROC curves were drawn and the AUCs were calculated and compared according to Hanley & McNeil.[41] The combination of MURs is calculated by a linear relationship of MURs1-3 derived from logistic regression: MURs = -2.16 + 0.32 × [MUR1] + 0.37 × [MUR2] + 0.17 × [MUR3], [MUR] indicates normalized fluorescence enhancement for the three MURs, respectively. All statistical calculations were performed using GraphPad Prism v.6 (GraphPad Software Inc., CA, USA).

Results and Discussion

Syntheses of MURs

The sensing mechanism of MURs1-3 are shown in Scheme 1. MUR1 is L-Glutamic acid γ-(7-amido-4-methylcoumarin), which is a specific GGT-activatable probe and emits blue fluorescence signals after enzymatic cleavage. MUR2 was derived from an orange-fluorescent dye, resorufin, by caging its optically tunable hydroxyl group with a self-immolative linker connected to AAP-cleavable alanine amino acid (Ala). Upon AAP cleavage at the terminal alanyl group, the linker is released by 1,6-immolation, leading to free resorufin unit with enhanced electron-donating ability from the oxygen atom. Similarly, MUR3 was synthesized from a NIR fluorescent hemicyanine dye (CyOH), with its hydroxyl group caged by a NAG-cleavable responsive group (N-acetyl-*β*-D-glucosaminide). In the presence of NAG, the terminal glycosidic bond is cleaved, forming free CyOH unit with enhanced electron-donating ability from the oxygen atom. Therefore, MURs2-3 are able to turn on their orange and NIR fluorescence signals in the presence of AAP and NAG, respectively.

MURs2-3 were synthesized through a synergistic approach (Scheme S1). The amino acid alanine was first coupled to p-aminobenzyl alcohol with subsequent 1º bromination to yield a highly active compound 2. Compound 2 was then conjugated to the hydroxyl group on resorufin followed by Fmoc deprotection on Alanyl amino group to afford MUR2. As for MUR3, its precursor CyOH was obtained by reacting IR775-Cl with resorcinol via a retro-Knoevenagel reaction. For its biomarker responsive compartment, a highly reactive compound 4 was afforded by brominating N-acetyl-*β*-D-glucosamine tetraacetate at its anomeric center, it was then reacted with the hydroxyl group of CyOH to afford compound 5, and compound 5 was deprotected of acetate groups to yield MUR3. The structures of these compounds were confirmed by NMR and mass spectra (Supporting Information).

In vitro detection

To investigate detection sensitivity and specificity of MURs, their UV-vis absorption and fluorescence spectra were measured in the absence or presence of biomarkers (Figure 1 and Table S1). Note that all MURs were barely fluorescent at their intrinsic states. After incubation of MUR1 with GGT, its absorption maximum shifted from 325 to 345 nm, and fluorescence signals at 440 nm enhanced 67-times (Figure 1a). Similarly, upon treatment of MUR2 with AAP, its absorption maximum shifted from 480 to 570 nm, which is the characteristic peak for released resorufin (Figure 1b). At this time point, MUR2 showed 60-fold fluorescence enhancement. Moreover, when MUR3 was incubated with NAG, its absorption maximum shifted from 600 to 690 nm, due to enzymatic cleavage at the ester bond and generation of free CyOH unit (Figure 1c). Meanwhile, MUR3 showed 33-fold fluorescence enhancement. High-performance liquid chromatography (HPLC) analysis confirmed that in the presence of their respective biomarkers, MURs1-3 were totally converted into the free fluorescent dyes AMC (quantum yield, Φ_f = 0.70), resorufin (Φ_f = 0.39), and CyOH (Φ_f = 0.21), respectively (Figure 1d-f). All MURs showed negligible fluorescence changes in the presence of interfering enzymes (Figure 1g-i). Besides, the catalytic efficiencies of GGT, AAP and NAG towards MURs1-3 were respectively calculated to be 31.8, 0.24 and 0.0198 $\mu M^{-1}s^{-1}$, and linear relationships existed between fluorescence intensity and the concentration of biomarkers (Figure S1 and Table S2).

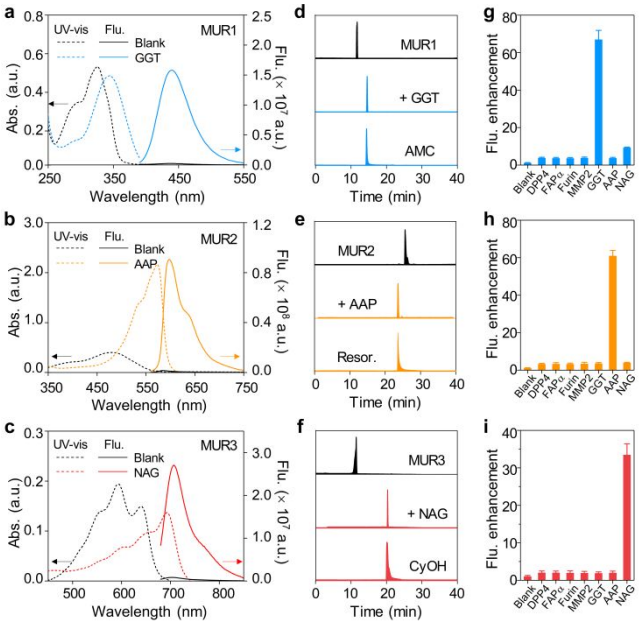

Figure 1. Evaluation of MURs sensing capabilities. (a-c) UV-vis absorption and fluorescence spectra of MURs1-3 (20 μM) in the absence or presence of their respective biomarkers (0.8 μg/mL GGT, 0.8 μg/mL AAP and 60 mU/mL NAG) in PBS (10mM, pH = 7.4 with 0.02% Tween@20), Tris (50 mM, pH = 7.4) and PBS (10mM, pH = 7.4), respectively. (d-f) HPLC traces of MURs1-3 in the absence or presence of their respective biomarkers, and traces of pure AMC (7-amino-4-methylcoumarin), resorufin and CyOH. (g-i) Fluorescence signal changes of MUR1 (440 nm), MUR2 (590 nm) and MUR3 (710 nm) relative to the blank in the presence of different enzymes. Error bars are standard deviation from three separate measurements. Fibroblast activation protein-alpha (FAPα), matrix metalloproteinase-2 (MMP2), dipeptidyl peptidase-4 (DPP4).

MURs cocktail multiplex imaging

To test the capability of MURs for multiplex imaging, MUR1-3 were mixed at an optimized equimolar ratio (MURs cocktail) and the fluorescence spectra was measured in the absence or presence of all three biomarkers by selective excitation at their respective absorption wavelengths (380, 550, and 670 nm). Upon excitation at 380 nm, only fluorescence signal of MUR1 at 440nm was detected, but signals of MURs2-3 were negligible. This was attributed to the absence of fluorescence resonance energy transfer (FRET) among MURs, because individual MUR molecules were free and away from each other in solutions and their spectra had minimal overlap. Similar spectral behaviours were upon excitation at 550 or 670 nm, only showing the signal of MUR2 or MUR3. Thus, the MURs cocktail could realize simultaneous detection of these biomarkers with minimal signal interference (Figure 2a).

The MURs cocktail was then used for multiplex imaging of endogenous biomarkers in kidney proximal tubule epithelial cells (HK-2) after confirming their low cytotoxicity in living cells (Figure S2). Compared to normal

dermal fibroblasts (NDF) as control, the fluorescence intensities of MURs1-3 in HK-2 were ~20-times higher, because of the high expression levels of these enzymes in HK-2 cells (Figure 2b-c). These results confirmed the feasibility of MURs cocktail for multiplex fluorescence imaging of multiple biomarkers.

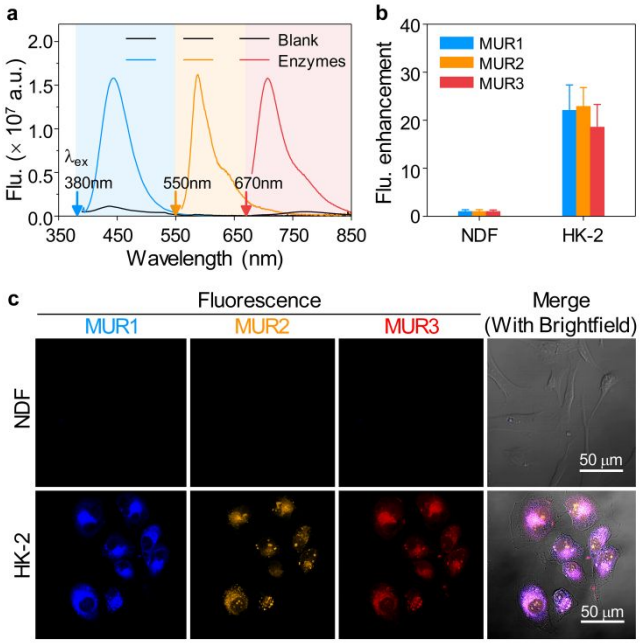

Figure 2. Multiplex fluorescence imaging in solution and renal cells. (a) Fluorescence spectra of MURs cocktail (containing 15 μM of each MUR) in the absence or presence of all three biomarkers–GGT, AAP and NAG in PBS (1×, pH = 7.4) containing 5% DMSO. Arrows indicate respective excitation wavelength for MURs1-3. (b) Fluorescence intensity enhancement of single HK-2 relative to NDF cells in Figure 2c (n = 3, mean ± s.d.). (c) Multiplex fluorescence images of human primary dermal fibroblasts (NDF) and kidney proximal tubule epithelial cells (HK-2) after incubation with MURs cocktail (containing 10 μM of each MUR).

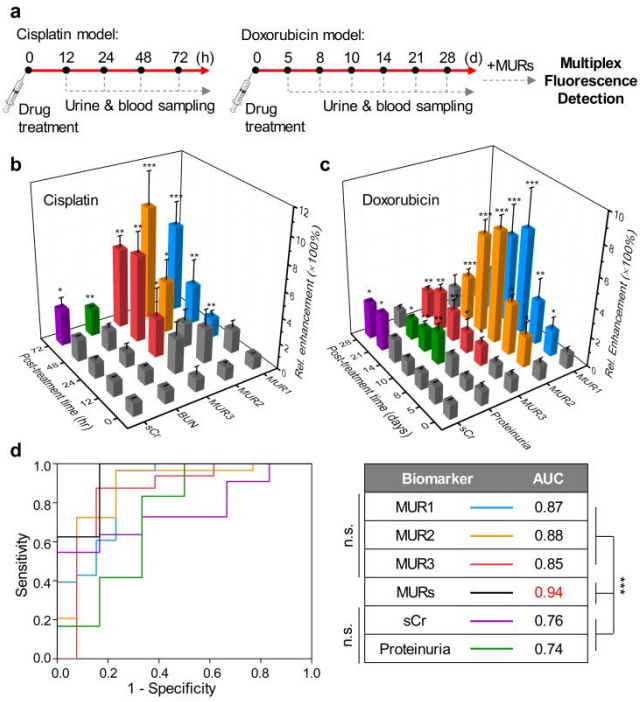

Figure 3. Multiplex urinalysis for detection of DIKI. (a) Timeline for development of cisplatin and doxorubicin–induced kidney injury. Mice were treated with cisplatin (intraperitoneal injection, 20 mg/kg bw) or doxorubicin (intravenous injection, 10 mg/kg bw), and urine samples that were collected from drug-treated mice at indicated post-treatment timepoints were then incubated with MURs cocktail (containing 10 μM of each MUR) for 1 h at 37 ºC in PBS (1×, pH = 7.4) containing 5% DMSO. Commercial assays were used to measure Cr, BUN in serum and proteinuria in urine. (b-c) Fluorescence enhancement of MURs1-3 after incubation with urine samples collected from drug-treated living mice, and fold changes in urinary and serum biomarkers at different post-treatment times. *Statistically significant difference in fluorescence enhancement and biomarkers fold change between pre-treatment and indicated statistically significant timepoints post-treatment of drugs. (n=5, mean ± s.d.) (d) ROC curves for the exclusion analysis (nephrotoxicant-treated animals with observed renal injuries versus animals not-treated with nephrotoxicant and without renal injuries) with the two nephrotoxicant studies. MURs is linear combination of MURs1-3 derived from logistic regression. (kidney injury [n = 28] vs control [n = 13]) n.s.: not significant; *p<0.05; **p<0.01; ***p<0.001.

Multiplex Optical Urinalysis

After confirming their plasma stability (Figure S3), MURs were then used to detect urinary biomarkers in murine models of DIKI with two nephrotoxicants – cisplatin and doxorubicin. Cisplatin is an antineoplastic drug with side effects of acute kidney injury (AKI), which is characterized by sequential physiological events: acute tubular necrosis, rapid GFR decline and kidney dysfunction.[42] Differently, doxorubicin-induced kidney injury is a mouse model that mimics human chronic kidney disease (CKD) caused by focal segmental glomerulosclerosis.[43] Specifically, healthy mice received one-time drug treatment of cisplatin (20 mg/kg bw) or doxorubicin (10 mg/kg bw) (Figure 3a). At different post-treatment timepoints, urine and blood samples were collected, and mice were sacrificed to collect

kidneys for histological analysis. The urine samples were incubated with MURs cocktail before multiplex fluorescence analysis, and serum biomarkers were tested using commercial assays. In the context of CKD, proteinuria was also tested as a clinical urinary biomarker reflecting glomerulosclerosis.[44]

In the cisplatin-induced AKI model, the first statistically significant fluorescence enhancement of MURs1-3 was observed at 24 (1.52-fold), 48 (4.05-fold) and 24 h (3.02-fold), respectively (Figure 3b and Figure S4). In contrast, the statistically significant increase of serum sCr and BUN was observed at a later timepoint, 72 h (2.81 & 2.15-fold) after cisplatin treatment, when histological injuries like loss of brush border and renal cell debris could be readily observed (Figure S5). In the doxorubicin-induced CKD model, the first statistically significant fluorescence enhancement of MURs1-3 was observed at 5 (1.74-fold), 5 (2.06-fold) and 8 days (1.37-fold). Proteinuria and serum creatinine had statistically significant increase at later timepoints, 10 (2.17-fold) and 21 days (2.45-fold). Histological injuries were observed from 14 days onwards (Figure S6). Meanwhile, significant mice weight loss for cisplatin and doxorubicin- induced kidney injury models were observed at 48 h and 8 days, respectively (Figure S7). Thereafter, MURs1-3 detected cisplatin and doxorubicin-induced kidney injury at 24 h and 5 days post-treatment, which are respectively 48 h and 5 days earlier than traditional diagnostic methods including sCr, BUN and proteinuria. The differences in statistically significant timepoints among MURs1-3 could be probably attributed to the biomarkers' individual regulation pathways in renal cells after drug challenge.

In order to quantitatively study the diagnostic performance (sensitivity and specificity), receiver operating characteristic (ROC) exclusion analysis was conducted by comparing the diagnosis results of MURs between two groups – healthy mice without histology injuries and drug-treated mice with obvious histology injuries. Besides, the area under curve (AUC) has statistical meaning of diagnostic accuracy and enables comparison between MURs and traditional diagnostic methods. MURs1-3 showed significantly higher AUC (≥ 0.85) compared with the tested traditional diagnostic approaches (AUC ~ 0.75). However, the performance differences among MURs1-3 were not statistically significant. Additionally, combination of MURs1-3 had the highest AUC (0.94), proving the better diagnostic performance than the individual MURs and the tested traditional clinical diagnostic measures. Thus, MURs were competent for early and accurate diagnosis of DIKI in both acute and chronic injuries.

Conclusions

In conclusion, we have developed molecular urinary reporters (MURs) and demonstrated their potential as the cocktail sensor in early detection of DIKI in mouse models. MURs1-3 sensitively and specifically turned on their fluorescence signals in the presence of their respective urinary biomarkers. Because MURs has minimum spectral overlap, they served as a cocktail for multiplex detection of three urinary biomarkers in both living renal cells and the mouse urine samples. In particularly, MURs detected cisplatin-induced AKI and doxorubicin-induced CKD at 24 h and 5 days after drug challenge, which were respectively 48 h and 5 days earlier than tested clinical diagnostic methods. Furthermore, an ROC exclusion analysis highlighted that MURs had better diagnostic accuracy than traditional diagnostic methods. However, in this study, MURs are only tested in drug-induced kidney injury models. To further validate the specificity of MURs, future studies should be conducted to include urine samples from patients with some common diseases like diabetes, cardiovascular disease, and other urinary disease like bladder cancer. Thus, this study exemplified a pioneering multiplex molecular detection method with a great potential for real-time monitoring of kidney function in preclinical drug screening and clinical diagnosis.

ASSOCIATED CONTENT

Supporting Information

The Supporting Information is available free of charge on the ACS Publications website.

Supporting Information. Supporting Figures and Tables (PDF).

AUTHOR INFORMATION

Corresponding Author

Kanyi Pu – School of Chemical and Biomedical Engineering, Nanyang Technological University, 637457 Singapore. Email: kypu@ntu.edu.sg

Notes

The authors declare no competing financial interest.

ACKNOWLEDGMENT

K.P. thanks Nanyang Technological University (Start-Up grant: M4081627), Singapore Ministry of Education Academic Research Fund Tier 1 (2017-T1-002-134, RG147/17; 2019-T1-002-045, RG125/19), and Academic Research Fund Tier 2 (MOE2018-T2-2-042) for the financial support.

REFERENCES

(1) Choudhury, D.; Ahmed, Z. Drug-associated renal dysfunction and injury. *Nat. Clin. Pract. Nephrol.* **2006**, 2, 80-91.

(2) Network, V. N. A. R. F. T. Intensity of renal support in critically ill patients with acute kidney injury. *N. Engl. J. Med.* **2008**, *359*, 7-20.

(3) Kellum, J. A.; Prowle, J. R. Paradigms of acute kidney injury in the intensive care setting. *Nat. Rev. Nephrol.* **2018**, *14*, 217-230.

(4) Darmon, M.; Ostermann, M.; Cerda, J.; Dimopoulos, M. A.; Forni, L.; Hoste, E.; Legrand, M.; Lerolle, N.; Rondeau, E.; Schneider, A.; Souweine, B.; Schetz, M. Diagnostic work-up and specific causes of acute kidney injury. *Intensive Care Med* **2017**, *43*, 829-840.

(5) Waikar, S. S.; Bonventre, J. V. Creatinine kinetics and the definition of acute kidney injury. *J. Am. Soc. Nephrol.* **2009**, *20*, 672-679.

(6) Baxmann, A. C.; Ahmed, M. S.; Marques, N. C.; Menon, V. B.; Pereira, A. B.; Kirsztajn, G. M.; Heilberg, I. P. Influence of muscle mass and physical activity on serum and urinary creatinine and serum cystatin C. *Clin. J. Am. Soc. Nephrol.***2008**, *3*, 348-354.

(7) Dieterle, F.; Perentes, E.; Cordier, A.; Roth, D. R.; Verdes, P.; Grenet, O.; Pantano, S.; Moulin, P.; Wahl, D.; Mahl, A. Urinary clusterin, cystatin C, β2-microglobulin and total protein as markers to detect drug-induced kidney injury. *Nat. Biotechnol.*, **2010**, *28*, 463-469.

(8) Noto, A.; Ogawa, Y.; Mori, S.; Yoshioka, M.; Kitakaze, T.; Hori, T.; Nakamura, M.; Miyake, T. Simple, Rapid Spectrophotometry of

Urinary N-Acetyl-Beta-D-Glucosaminidase, with Use of a New Chromogenic Substrate. *Clin. Chem.* **1983**, *29*, 1713-1716.

(9) Duncan, M. W.; Nedelkov, D.; Walsh, R.; Hattan, S. J. Applications of MALDI Mass Spectrometry in Clinical Chemistry. *Clin. Chem.* **2016**, *62*, 134-143.

(10) Zhang, Y.; Wang, D.; Goel, S.; Sun, B.; Chitgupi, U.; Geng, J.; Sun, H.; Barnhart, T. E.; Cai, W.; Xia, J.; Lovell, J. F. Surfactant-Stripped Frozen Pheophytin Micelles for Multimodal Gut Imaging. *Adv. Mater.* **2016**, *28*, 8524-8530.

(11) Wang, H.; Feng, Z.; Del Signore, S. J.; Rodal, A. A.; Xu, B. Active Probes for Imaging Membrane Dynamics of Live Cells with High Spatial and Temporal Resolution over Extended Time Scales and Areas. *J. Am. Chem. Soc.* **2018**, *140*, 3505-3509.

(12) Huang, J.; Pu, K. Activatable Molecular Probes for Second Near-Infrared Fluorescence, Chemiluminescence, and Photoacoustic Imaging. *Angew. Chem., Int. Ed.*, **2020.** DOI: 10.1002/anie.202001783

(13) Kwok, R. T.; Leung, C. W.; Lam, J. W.; Tang, B. Z. Biosensing by luminogens with aggregation-induced emission characteristics. *Chem. Soc. Rev.* **2015**, *44*, 4228-4238.

(14) Lovell, J. F.; Liu, T. W.; Chen, J.; Zheng, G. Activatable photosensitizers for imaging and therapy. *Chem. Rev.* **2010**, *110*, 2839-2857.

(15) Yang, Y.; Zhao, Q.; Feng, W.; Li, F. Luminescent chemodosimeters for bioimaging. *Chem. Rev.* **2013**, *113*, 192-270.

(16) Ren, C.; Zhang, J.; Chen, M.; Yang, Z. Self-assembling small molecules for the detection of important analytes. *Chem. Soc. Rev.* **2014**, *43*, 7257-7266.

(17) Xiao, M.; Sun, W.; Fan, J.; Cao, J.; Li, Y.; Shao, K.; Li, M.; Li, X.; Kang, Y.; Zhang, W.; Long, S.; Du, J.; Peng, X. Aminopeptidase-N-activated Theranostic Prodrug for NIR Tracking of Local Tumor Chemotherapy. *Adv. Funct. Mater.* **2018**, *28*, 1805128.

(18) Li, Q.; Li, S.; He, S.; Chen, W.; Cheng, P.; Zhang, Y.; Miao, Q.; Pu, K. Activatable Polymeric Reporter For Near-infrared Fluorescent and Photoacoustic Imaging of Invasive Cancer. *Angew. Chem., Int. Ed.*, **2020**, DOI: 10.1002/anie.202000035.

(19) He, S.; Li, J.; Lyu, Y.; Huang, J.; Pu, K. Near-Infrared Fluorescent Macromolecular Reporters for Real-Time Imaging and Urinalysis of Cancer Immunotherapy. *J. Am. Chem. Soc.* **2020**. DOI: 10.1021/jacs.0c00659

(20) Huang, J.; Jiang, Y.; Li, J.; He, S.; Huang, J.; Pu, K. A Renal-Clearable Macromolecular Reporter for Near-Infrared Fluorescence Imaging of Bladder Cancer. *Angew. Chem., Int. Ed.*, **2020**, *59*, 4415-4420.

(21) Cheng, P.; Zhang, J.; Huang, J.; Miao, Q.; Xu, C.; Pu, K. Near-infrared fluorescence probes to detect reactive oxygen species for keloid diagnosis. *Chem. Sci.* **2018**, *9*, 6340-6347.

(22) Miao, Q.; Yeo, D. C.; Wiraja, C.; Zhang, J.; Ning, X.; Xu, C.; Pu, K. Near-Infrared Fluorescent Molecular Probe for Sensitive Imaging of Keloid. *Angew. Chem., Int. Ed.*, **2018**, *57*, 1256-1260.

(23) Miao, Q. Q.; Xie, C.; Zhen, X.; Lyu, Y.; Duan, H. W.; Liu, X. G.; Jokerst, J. V.; Pu, K. Y. Molecular afterglow imaging with bright, biodegradable polymer nanoparticles. *Nat. Biotechnol.* **2017**, *35*, 1102-1110.

(24) Shuhendler, A. J.; Pu, K. Y.; Cui, L.; Uetrecht, J. P.; Rao, J. H. Real-time imaging of oxidative and nitrosative stress in the liver of live animals for drug-toxicity testing. *Nat. Biotechnol.* **2014**, *32*, 373-380.

(25) Cheng, P.; Miao, Q.; Li, J.; Huang, J.; Xie, C.; Pu, K. Unimolecular chemo-fluoro-luminescent reporter for crosstalk-free duplex imaging of hepatotoxicity. *J. Am. Chem. Soc.* **2019**, *141*, 10581-10584.

(26) Yang, M.; Fan, J.; Zhang, J.; Du, J.; Peng, X. Visualization of methylglyoxal in living cells and diabetic mice model with a 1,8-naphthalimide-based two-photon fluorescent probe. *Chem. Sci.* **2018**, *9*, 6758-6764.

(27) Zhou, L.; Fan, Y.; Wang, R.; Li, X.; Fan, L.; Zhang, F. High-Capacity Upconversion Wavelength and Lifetime Binary Encoding for Multiplexed Biodetection. *Angew. Chem., Int. Ed.* **2018**, *57*, 12824-12829.

(28) Heinzmann, K.; Carter, L. M.; Lewis, J. S.; Aboagye, E. O. Multiplexed imaging for diagnosis and therapy. *Nat. Biomed. Eng.* **2017**, *1*, 697.

(29) Yan, F.; Tian, X.; Luan, Z.; Feng, L.; Ma, X.; James, T. D. NAG-targeting fluorescence based probe for precision diagnosis of kidney injury. *Chem. Comm.* **2019**, *55*, 1955-1958.

(30) Huang, J.; Lyu, Y.; Li, J.; Cheng, P.; Jiang, Y.; Pu, K. A Renal-Clearable Duplex Optical Reporter for Real-Time Imaging of Contrast-Induced Acute Kidney Injury. *Angew. Chem., Int. Ed.*, **2019**, *131*, 17960-17968.

(31) Huang, J.; Xie, C.; Zhang, X.; Jiang, Y.; Li, J.; Fan, Q.; Pu, K. Renal-clearable Molecular Semiconductor for Second Near-Infrared Fluorescence Imaging of Kidney Dysfunction. *Angew. Chem., Int. Ed.*, **2019**, *58*, 15120-15127.

(32) Jung, K.; Schulze, B.-D.; Sydow, K. Diagnostic significance of different urinary enzymes in patients suffering from chronic renal diseases. *Clin. Chim. Acta* **1987**, *168*, 287-295.

(33) Malhotra, R.; Siew, E. D. Biomarkers for the early detection and prognosis of acute kidney injury. *Clin. J. Am. Soc. Nephro.* **2017**, *12*, 149-173.

(34) Luo, Z.; Huang, Z.; Li, K.; Sun, Y.; Lin, J.; Ye, D.; Chen, H.-Y. Targeted delivery of a γ-glutamyl transpeptidase activatable near-infrared-fluorescent probe for selective cancer imaging. *Anal. Chem.* **2018**, *90*, 2875-2883.

(35) Li, L.; Shi, W.; Wu, X.; Gong, Q.; Li, X.; Ma, H. Monitoring γ-glutamyl transpeptidase activity and evaluating its inhibitors by a water-soluble near-infrared fluorescent probe. *Biosens. Bioelectron.* **2016**, *81*, 395-400.

(36) Cheng, P.; Chen, W.; Li, S.; He, S.; Miao, Q.; Pu, K. Fluoro-Photoacoustic Polymeric Renal Reporter for Real-Time Dual Imaging of Acute Kidney Injury. *Adv. Mater.* **2020**, 1908530.

(37) He, X.; Xu, Y.; Shi, W.; Ma, H. Ultrasensitive Detection of Aminopeptidase N Activity in Urine and Cells with a Ratiometric Fluorescence Probe. *Anal. Chem.* **2017**, *89*, 3217-3221.

(38) Yan, F.; Tian, X.; Luan, Z.; Feng, L.; Ma, X.; James, T. D. NAG-targeting fluorescence based probe for precision diagnosis of kidney injury. *Chem. Comm.* **2019**, *55*, 1955-1958.

(39) Huang, J.; Li, J.; Lyu, Y.; Miao, Q.; Pu, K. Molecular optical imaging probes for early diagnosis of drug-induced acute kidney injury. *Nat. Mater.* **2019**, 18, 1133-1143.

(40) Yuan, L.; Lin, W.; Zhao, S.; Gao, W.; Chen, B.; He, L.; Zhu, S. A unique approach to development of near-infrared fluorescent sensors for in vivo imaging. *J. Am. Chem. Soc.* **2012**, *134*, 13510-13523.

(41) Hanley, J. A.; McNeil, B. J. A method of comparing the areas under receiver operating characteristic curves derived from the same cases. *Radiology* **1983**, *148*, 839-843.

(42) Singh, A. P.; Junemann, A.; Muthuraman, A.; Jaggi, A. S.; Singh, N.; Grover, K.; Dhawan, R. Animal models of acute renal failure. *Pharmacol. Rep.* **2012**, *64*, 31-44.

(43) Wang, Y.; Wang, Y. P.; Tay, Y. C.; Harris, D. C. Progressive adriamycin nephropathy in mice: sequence of histologic and immunohistochemical events. *Kidney Int.* **2000**, *58*, 1797-1804.

(44) Fassett, R. G.; Venuthurupalli, S. K.; Gobe, G. C.; Coombes, J. S.; Cooper, M. A.; Hoy, W. E. Biomarkers in chronic kidney disease: a review. *Kidney Int.* **2011**, *80*, 806-821.

For Table of Contents only.

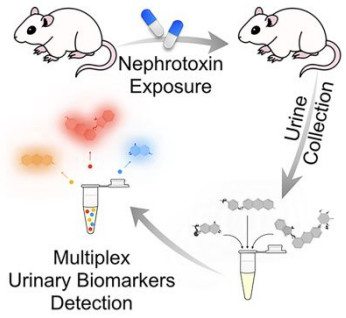
Nephrotoxin
Exposure
Urine
Collection
Multiplex
Urinary Biomarkers
Detection